Chinese Chemical Letters 37 (2026) 111078

Contents lists available at ScienceDirect

Chinese Chemical Letters

journal homepage: www.elsevier.com/locate/cclet

Hydrogen bonding-reinforced multi-component cross-linked hydrogel electrolytes with high ionic conductivity and stretchability for stabilized zinc anodes

Yu Wang, Kun Ding*, Xuerong Gong, Shou Chen, Ao Sun, Junxi Zhang, Baofeng Wang*

Shanghai Key Laboratory of Materials Protection and Advanced Materials in Electric Power, Shanghai University of Electric Power, Shanghai 200090, China

ARTICLE INFO

Article history:
Received 17 January 2025
Revised 27 February 2025
Accepted 12 March 2025
Available online 12 March 2025

Keywords:
Zn-ion batteries
Hydrogel electrolytes
Zn anode
Dendrites
Solvation structure

ABSTRACT

Hydrogel electrolytes are widely used in zinc-ion batteries (ZIBs) due to their advantages of regulating zinc deposition/stripping process, and limiting dendrite growth. However, their relatively poor ionic conductivity and mechanical properties remain significant obstacles to their practical application in ZIBs. Herein, the multi-component cross-linked polyacrylamide/carboxymethyl cellulose/agarose (PCA) hydrogel polymerized electrolytes are designed *via* a heat-initiated polymerization approach. The PCA hydrogel electrolytes exhibit high ionic conductivity of 38.78 mS/cm and excellent mechanical strength from 2.9 MPa to 5.6 MPa. Meanwhile, the ample hydroxyl (-OH) functional groups on the PCA hydrogel electrolytes chain can capture and anchor H_2O molecules *via* hydrogen bonding, thus fundamentally regulating the coordination environment of Zn^{2+} and inhibiting side reactions. The combined effect of carboxyl (-COOH) groups and amino (-NH_2) groups in PCA hydrogel electrolytes can induce the uniform deposition of zinc ions. Consequently, The Zn//Zn symmetrical cell assembled with this hydrogel electrolytes demonstrate excellent cycling stability over 2500 h at the current density of 1 mA/cm^2. Furthermore, the Zn//MnO_2/CNT full cell retains a specific capacity of 127.2 mAh/g after 1000 cycles at 1 A/g, with 97.8 % capacity retention.

© 2026 Published by Elsevier B.V. on behalf of Chinese Chemical Society and Institute of Materia Medica, Chinese Academy of Medical Sciences.

To achieve carbon peaking and carbon neutrality targets, the development of sustainable rechargeable batteries is urgently needed for high-performance energy storage systems [1–3]. In recent years, ZIBs have gained widespread interest due to their inherent safety, low redox potential (−0.76 V *vs.* standard hydrogen electrode), and high theoretical capacity (5854 mAh/cm^3) [4,5]. However, ZIBs face severe challenges related to the Zn-metal anode [*e.g.*, dendrite formation, Zn corrosion, and hydrogen evolution reaction (HER)] during the plating/stripping process, inevitably leading to poor reversibility and even short-circuited failure [6]. Various effective strategies have been exploited to overcome these obstacles, exemplified with artificial interface modification [7,8], structural optimization [9,10], electrolyte regulation [11–13] and using hydrogel electrolytes [14,15]. Among them, hydrogel electrolytes are the most attractive because they can effectively regulate interfacial ion transport, modulating the Zn deposition/stripping processes, limiting dendrite growth, and preventing the leakage of liquid electrolytes to ensure safety [16].

Hydrogel electrolyte is a polymer network formed by the covalent bonds (*e.g.*, -COO-, C=C) or hydrogen bonds (*e.g.*, -N···H, -O···H). The polar functional groups, such as -OH and -COOH, have garnered significant attention for their application in gel-state electrolytes [17,18]. These polar groups facilitate strong interactions with ionic species, enhancing ion dissociation and transport. This is critical for achieving high ionic conductivity in the hydrogel electrolytes, while fixing water molecules in the polymer framework and reduce side reactions so as to achieve uniform Zn deposition [19–21]. Besides, the hydrogel electrolyte can also increase the energy density of the battery due to its excellent water retention and broadened electrochemical window, and ultimately greatly prolong the service life of flexible Zn-based devices [22]. Typically, single network architectures like polyvinyl alcohol (PVA) [23], polyacrylamide (PAM) [24] and polyethylene glycol (PEG) [25] are utilized to construct commonly used hydrogel electrolytes. However, the mechanical properties of these single network hydrogel electrolytes are unsatisfactory to inhibit the growth of dendrites, resulting in a short circuit in the flexible battery under external forces [26]. Besides, the conventional single network hydrogel electrolyte possesses poor ionic conductivity, limiting its electrochemical performance.

* Corresponding authors.
E-mail addresses: kunding@shiep.edu.cn (K. Ding), wangbaofeng@shiep.edu.cn (B. Wang).

https://doi.org/10.1016/j.cclet.2025.111078
1001-8417/© 2026 Published by Elsevier B.V. on behalf of Chinese Chemical Society and Institute of Materia Medica, Chinese Academy of Medical Sciences.

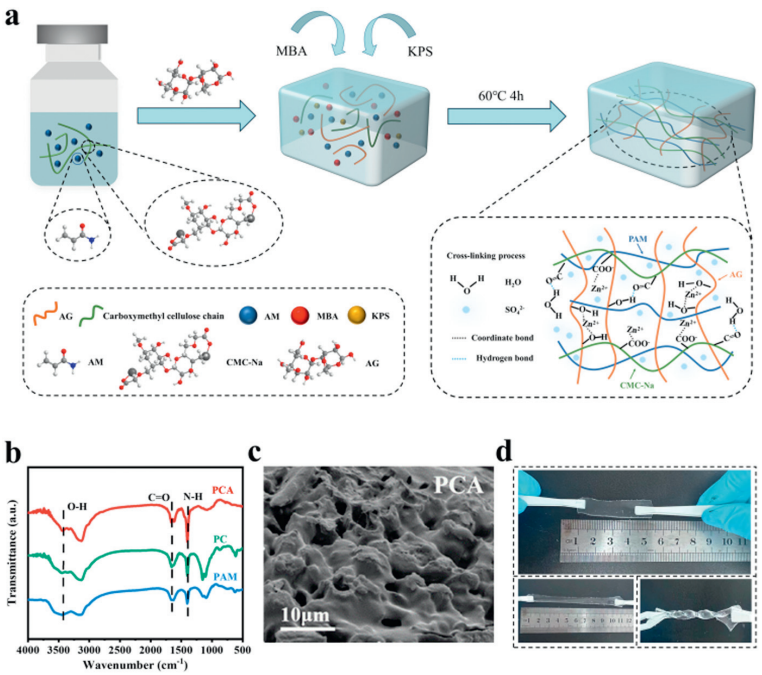


Fig. 1. (a) Schematic diagram of the preparation process of PCA hydrogel electrolytes. (b) FTIR spectra of different hydrogel samples. (c) SEM image of freeze-dried PCA hydrogel. (d) Digital images of the PCA hydrogel under stretching and twisting.

Some researchers have proposed a double-network hydrogel electrolyte with the introduction of a second network on top of the first network, where the first network is a rigid structure and the second network is loosely structured to increase the toughness [27]. It not only enhances the mechanical properties of the hydrogel, but also increases the ion transfer channels, resulting in better ion transport properties. Mao *et al.* constructed a CMC/PAM double network hydrogel electrolyte which improved the ionic conductivity and mechanical properties [28]. Therefore, it is crucial to develop hydrogel electrolytes with good mechanical properties and high ionic conductivity, as well as the ability to inhibit Zn dendrites and side reactions, in order to meet the demand for high-performance zinc ion batteries.

In this work, a multi-component cross-linked hydrogel electrolyte PCA polymerized by PAM, carboxymethyl cellulose (CMC), and agarose (AG) was designed by using thermal initiation polymerization method. The three-dimensional network structure endows the PCA hydrogel electrolytes with excellent mechanical strength and high ionic conductivity of 38.78 mS/cm. The -COOH in CMC induce the uniform deposition of Zn^{2+} on the (002) crystal surface, inhibiting the formation of zinc dendrites. The abundant -OH in PCA hydrogel electrolytes can form hydrogen bonds with water, reducing the free water content and weakening the activity of water molecules, thereby regulating the solvation structure of zinc ions and effectively suppressing zinc dendrite growth while alleviating side reactions. Consequently, the Zn//Zn symmetrical battery assembled with the PCA hydrogel electrolytes exhibits a cycling life of 2500 h. The Zn//Cu asymmetric cells demonstrate nearly 98.6 % Coulombic efficiency (CE) over 350 cycles. Furthermore, the Zn//MnO_2/CNT full cells assembled with the PCA hydrogel electrolytes exhibit excellent cycle stability with a capacity retention of 97.8 % after 1000 cycles. This work offers a promising strategy for polymer hydrogel electrolytes for flexible ZIBs.

The schematic diagram illustrating the preparation of PCA hydrogel electrolytes is depicted in Fig. 1a. In the presence of the initiator KPS and the crosslinking agent MBA, the acrylamide monomer undergoes a polymerization reaction, resulting in the formation of PCA hydrogel electrolytes with a three-dimensional network structure through crosslinking with CMC and AG. As shown in Fig. 1b, the peaks observed around 1628 and 3445 cm^{-1} are attributed to the overlapping of asymmetric -NH_2/-OH stretching and carbonyl stretching modes, respectively. These peaks demonstrate the successful crosslink of CMC and PAM through physical entanglement and hydrogen bonds. The variations in peaks within the range of 3000–3700 cm^{-1} further confirm the formation of hydrogen bonds between the -OH in AG and the -NH_2 in PAM [29]. The characteristic absorption peaks of AG are observable in the range of 900–1250 cm^{-1}. The sharp and medium-intensity band at 1045 cm^{-1}, accompanied by a weak band at 1156 cm^{-1}, are both attributed to the vibration mode of the C–O-C bridge within the glycosidic linkage. To further verify the successful preparation of PCA hydrogel electrolytes, Raman spectroscopy characterizations were conducted (Fig. S1 in Supporting information). With the addition of CMC, the combined interaction between the -COOH and the -NH_2 in the PAM hydrogel electrolytes results in a slight shift in the peak at 1423 cm^{-1}. Additionally, upon incorporating AG, the peak shifts within the range of 3200–3400 cm^{-1}, indicating the formation of hydrogen bonds between the -OH in AG and the -NH_2 in PAM hydrogel electrolytes. Therefore, it can be deduced that the AM monomer successfully underwent a crosslinking polymerization reaction with the main chains of the other two polymers. This multi-component crosslinked hydrogel electrolytes possessed more continuous network structure with interconnected pore spaces (Fig. 1c). Consequently, the PCA hydrogel electrolytes exhibited excellent flexibility, enabling them to be stretched and twisted without experiencing significant fracture (Fig. 1d).

Due to the three-dimensional network structure contains in this hydrogel electrolytes, it can not only enhance mechanical properties but also create abundant ion transport channel [30,31]. As shown in Fig. 2a, the tensile strength of the PCA hydrogel reaches up to 21.9 kPa, significantly higher than the 3.2 kPa of the PAM hydrogel. Meanwhile, mechanical measurements indicate that the compressive stress increases from 2.9 MPa to 5.6 MPa (Fig. 2b),

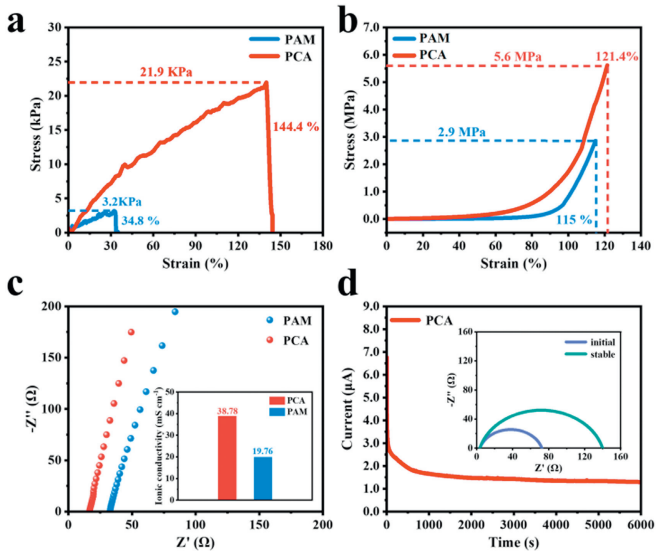


Fig. 2. (a) Tensile stress-strain curve of PCA and PAM hydrogel. (b) Compression stress-strain curves of PCA and PAM hydrogel. (c) Nyquist plots of PCA and PAM hydrogel (inset: the corresponding ionic conductivity). (d) *I-t* curve of Zn/PCA-hydrogel/Zn symmetric cell (inset: Nyquist plots before and after polarization).

demonstrating that the mechanical properties of the PCA hydrogel are markedly enhanced due to appropriate crosslinking. As shown in Fig. 2c, the ionic conductivity of PCA hydrogel electrolytes reaches up to 38.78 mS/cm, while that of the PAM hydrogel electrolytes is only 19.76 mS/cm, surpassing many reported hydrogel electrolytes (Table S1 in Supporting information). Notably, the PCA hydrogel electrolytes also exhibit a higher Zn^{2+} transference number of 0.58 compared to PAM hydrogel electrolytes (0.42) (Fig. 2d and Fig. S2 in Supporting information). A high ion transference number not only achieves low polarization by establishing a smaller concentration gradient but also allows facilitates uniform Zn deposition and high capacity in ZIBs [32].

The long-term stability in Zn//Cu asymmetric cells and Zn//Zn symmetric cells using different electrolytes were further explored. The Zn//Zn cells in PAM hydrogel electrolyte only survive around 600 h, and the lifespan of Zn//Zn cells in liquid electrolytes (LE) was as short as 100 h. However, the Zn//Zn cells in PCA hydrogel electrolytes exhibited excellent cycle stability of up to 2500 h (Fig. 3a), which surpasses that the most reported studies (Table S2 in Supporting information). At the same time, it was found that the Zn//Zn cells with PCA hydrogel electrolytes demonstrated superior cycling stability even at low current densities (Fig. S3 in Supporting information). As shown in Fig. 3b, the asymmetric Zn//Cu cells using LE exhibited a sharp decline in performance after approximately 70 cycles. The Zn anode in the PAM hydrogel electrolyte also fails to work after 150 cycles. In contrast, the PCA hydrogel electrolytes demonstrated outstanding reversible electrochemical performance, maintaining an average CE of 98.6 % over 350 cycles. This adequately demonstrating excellent reversibility and stability of Zn plating/stripping within the PCA hydrogel electrolytes. As shown in Fig. 3c, the voltage curves corresponding to the PCA hydrogel electrolytes are stable and highly overlapping, further confirming that the PCA hydrogel electrolytes enable an efficient and reversible zinc deposition/dissolution process.

The nucleation overpotential (NOP) for zinc deposition on titanium foil was tested using different electrolytes at a current density of 1 mA/cm^2. As shown in Fig. 3d, the NOP for the Zn//Ti cell using PCA hydrogel electrolytes was 60 mV, which is lower than the 74 mV for PAM and 92 mV for LE. This indicates that PCA hydrogel electrolytes provide more nucleation sites, which is advantageous for achieving quick and uniform Zn deposition when the nucleation overpotential is lower. Furthermore, the nucleation and deposition processes of Zn^{2+} were characterized using the chronoamperometry (CA) method. As shown in Fig. 3e, the current density sharply decreased within 150 s before stabilizing for LE. In contrast, the zinc electrode in PCA and PAM hydrogel electrolytes experienced only a brief decay period (within 20 s) before reaching a stable 3D compact diffusion process. The continuously lower and stable current density after 2D diffusion in PCA hydrogel electrolytes suggests that Zn ions tend to deposit on the initial absorption sites and form the smooth surface on Zn anode. The diffusion behavior variation should be initiated by the promoted Zn^{2+} diffusion by the carboxylic groups in PCA hydrogel electrolytes, which would be expected to benefit a smoother and slower deposition of Zn complexes along 3D diffusion pathways. Fig. S4 (Supporting information) shows the EIS profiles of the symmetric cells under various temperatures (ranging from 25 °C to 65 °C). The R_{ct} of the PCA hydrogel electrolyte remains consistently lower than those of PAM and LE electrolytes at various temperatures, indicating that the PCA hydrogel electrolyte possesses favorable interfacial compatibility. Notably, compared to LE and PAM electrolytes, the E_a of PCA hydrogel electrolytes is obviously reduced, which suggests that the PCA hydrogel electrolytes enable a fast desolvation process of the solvated Zn^{2+} ions for accelerating the Zn deposition kinetics (Fig. 3f) [33]. As demonstrated by Tafel curves in Fig. 3g, the PCA hydrogel electrolytes can effectively restrain the corrosion reaction of Zn anodes, exhibiting the lower corrosion current (I_{corr}) of 0.76 mA/cm^2 compared to PAM hydrogel electrolytes (0.97 mA/cm^2) and LE (1.23 mA/cm^2). These results indicate that the PCA hydrogel electrolytes can effectively achieve stable and uniform zinc deposition, leading to highly stable cycling performance in ZIBs.

The inhibition of Zn dendrite formation and corrosion by PCA hydrogel electrolytes is visualized in Figs. 4a-c using SEM. After 100 charging/discharging cycles in the PCA hydrogel electrolytes, almost no significant dendrite formation was observed, and the surface of the zinc anode remained very flat. In the PAM hydrogel electrolytes, the surface of the zinc anode exhibited notable cracks and depressions, resulting in a small amount of zinc dendrites. In LE, a large number of disordered and sharp zinc dendrites were clearly visible on the surface of the zinc anode. To more intuitively compare the side reactions of the zinc anode in different electrolytes, EDS tests were performed on the cross-sections (Figs. S5-S7 in Supporting information). The results showed that the sulfur and oxygen content in the PCA hydrogel electrolyte is significantly lower than that in the LE and PAM electrolytes. These findings further demonstrate that PCA hydrogel electrolytes effectively guide uniform zinc deposition, inhibiting the growth of zinc dendrites and the occurrence of side reactions.

To investigate the inhibition mechanism of solvation structures by PCA hydrogel electrolytes, Raman spectra of various electrolytes were characterized. As shown in Fig. 4d, the symmetric stretching vibration peaks of SO_4^{2-} were classified into contact ion pair CIP ($[Zn^{2+}(H_2O)_5OSO_3^{2-}]$) and solvent separated ion pair SIP ($[Zn^{2+}(H_2O)_6{\cdot}SO_4^{2-}]$). The CIP in PCA hydrogel electrolytes exhibited a significantly stronger intensity compared to that in PAM hydrogel electrolytes. This result demonstrated that PCA hydrogel electrolytes can modulate solvation structures, thereby altering the coordination environment of zinc ions to facilitate their migration and simultaneously reducing the activity of water molecules to inhibit side reactions. Fig. 4e displayed the FTIR spectra of different electrolytes. With the introduction of AG, the H–O bending vibration of free H_2O molecules shifted to higher wavenumbers (red-shift), indicating that -OH formed hydrogen bonds with water molecules, converting a significant amount of free water into bound water. This caused the water molecules to dissociate from the hydration shell of zinc ions [Zn $(H_2O)_6^{2+}$] and disrupted the

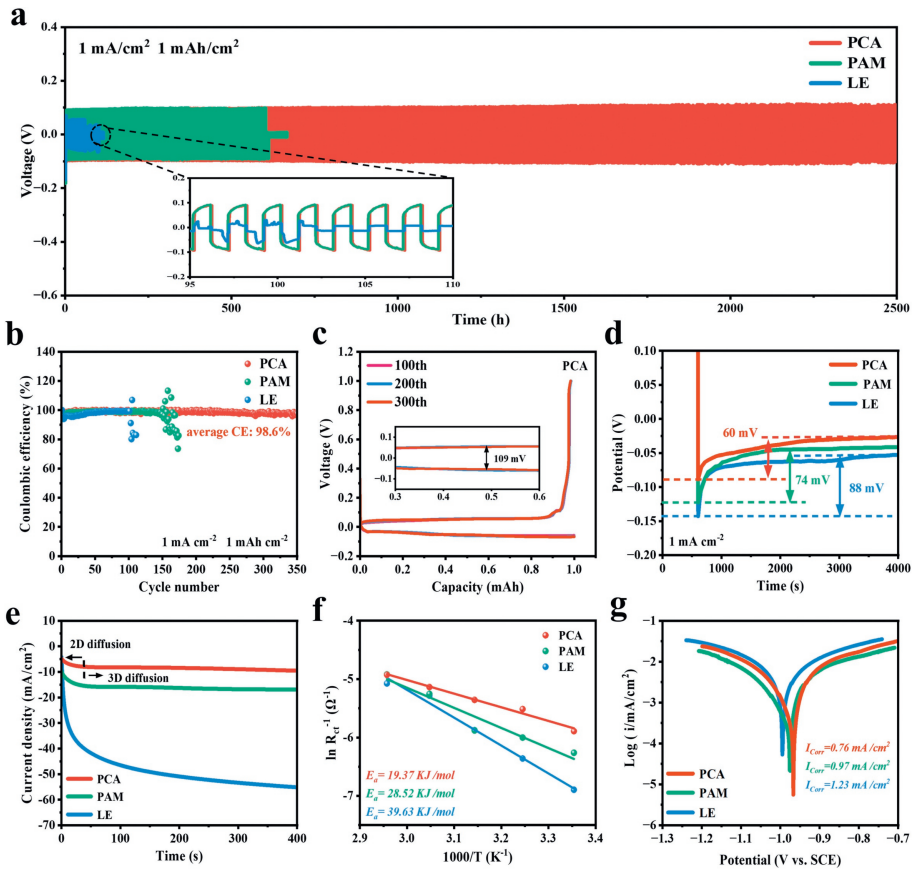


Fig. 3. (a) Voltage-time profiles of Zn//Zn symmetric cells with different electrolytes. (b) CE of Zn//Cu cells assembled with different electrolytes. (c) Voltage-capacity plots of Zn//Cu cells with PCA hydrogel electrolytes. (d) NOP of Zn deposition on titanium foil in different electrolytes. (e) CA curves with different electrolytes. (f) Comparison of the activation energies of different electrolytes. (g) Tafel curves with different electrolytes.

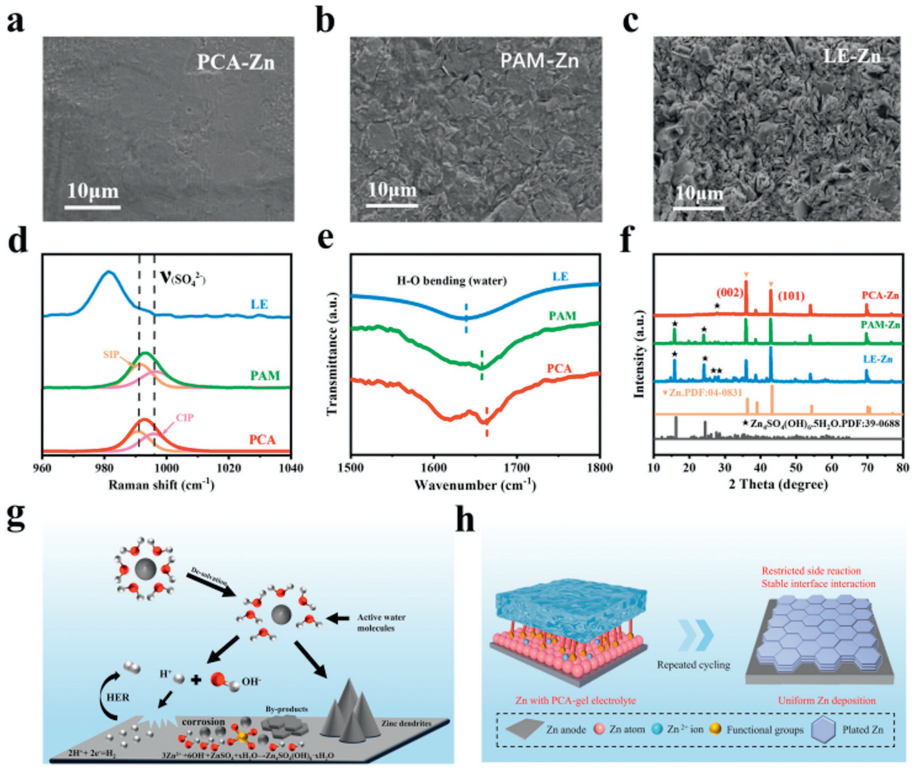


Fig. 4. (a) SEM images of the Zn electrodes after deposition/dissolution for 100 cycles in PCA hydrogel electrolytes. (b) PAM hydrogel electrolytes and (c) LE. (d) Raman and (e) FTIR spectra of different electrolytes. (f) XRD patterns of Zn electrodes after 100 charge/discharge cycles in different electrolytes. (g) Schematic illustration of Zn^{2+} solvation process and side reactions between zinc metal anode. (h) Schematic diagram of the mechanism of PCA hydrogel electrolytes acting on Zn anode surface.

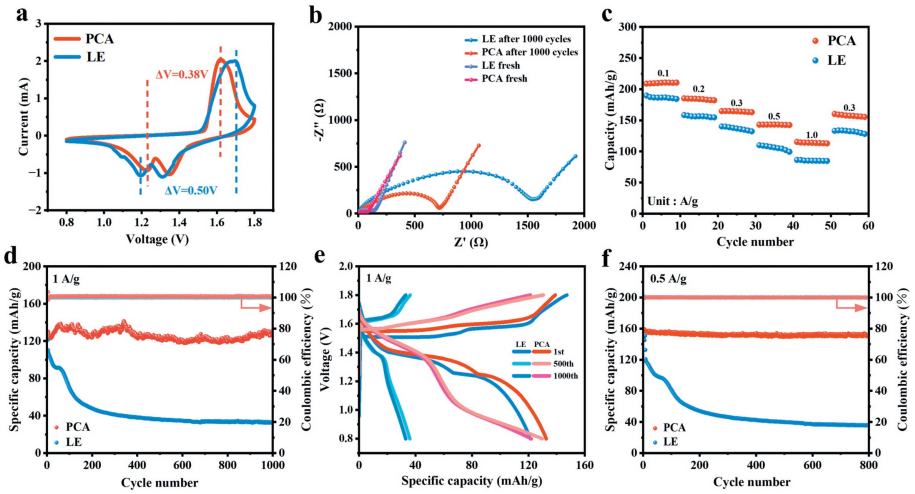


Fig. 5. (a) CV curves of Zn//MnO_2/CNT cells in LE and PCA electrolytes at the scan rate of 0.5 mV/s. (b) Nyquist plots before and after 1000 cycling. (c) Rate capability of full cells in LE and PCA electrolytes at various current densities. (d) Cycling performance at a current density of 1 A/g. (e) The corresponding charge/discharge curves at different cycle numbers. (f) Cycling performance at a current density of 0.5 A/g.

complexation structure between zinc ions and water molecules. Additionally, the evolution of hydrogen bonds in the electrolyte was further investigated *via* nuclear magnetic resonance (NMR) (Fig. S8 in Supporting information). The ^1H peak of the PCA hydrogel electrolyte shifts to a lower field, indicating a decrease in electron cloud density around the water molecules. This suggests that the hydroxyl groups in the PCA hydrogel electrolyte form a significant number of hydrogen bonds with water molecules, replacing the original hydrogen bonds between mobile water molecules. Therefore, the PCA hydrogel electrolytes effectively inhibited the growth of dendrites and the occurrence of side reactions. XRD analysis was performed on the by-products formed on the zinc anode. As shown in Fig. 4f, the zinc anode in the PCA hydrogel electrolytes corresponded to a pure Zn phase with no significant byproduct signals, suggesting that the PCA hydrogel electrolytes greatly reduced side reactions. Notably, zinc ions on the zinc anode in the PCA hydrogel electrolytes showed a clear tendency to deposit preferentially on the (002) crystal plane. Zn deposition on the (002) plane was more uniform and less prone to dendrite formation, as the (002) crystal plane was parallel to the zinc anode surface and had a lower binding energy. Consequently, the Zn deposition mechanism in LE and PCA electrolytes was concluded (Figs. 4g and h). Zinc ions form a solvated structure in LE and reactive water molecules on the surface of zinc electrodes are prone to participating in side reactions such as hydrogen precipitation and corrosion, leading to the growth of dendrites. On the contrary, in the PCA hydrogel electrolytes, the carboxyl groups guide the uniform deposition of zinc ions through electrostatic interactions, while the hydroxyl groups suppress the activity of water molecules *via* hydrogen bonding, reducing side reactions. The synergistic effect of these two functional groups enhances the uniformity of zinc deposition and the stability of the electrolyte, preventing the generation of by-products, thereby improving battery performance

As shown in Fig. 5a, the CV curves of the Zn//MnO_2/CNT cells exhibited typical redox reactions in both LE and PCA electrolytes over the voltage range of 0.8–1.8 V. The cells assembled with PCA hydrogel electrolytes showed higher redox current peaks and smaller polarization voltages compared to LE. EIS measurements indicated that the Zn//MnO_2/CNT cells with the PCA hydrogel electrolytes had lower charge transfer resistance before and after 1000 cycles (Fig. 5b). This result indicated the excellent electrochemical reversibility and rapid redox reaction kinetics provided by the PCA hydrogel electrolytes. Fig. 5c displays the rate performance of the Zn//MnO_2/CNT cells with LE and PCA electrolytes. In the PCA hydrogel electrolytes, the discharge capacity was maintained at 126 mAh/g at a current density of 1 A/g and also showed better recovery performance when the current density was restored to 0.3 A/g. Fig. 5d showed the full battery assembled with LE dropped rapidly with a capacity retention rate of 30.3 % after 100 cycles. In contrast, the PCA-assembled cell still retained a high specific capacity (127.2 mAh/g) after 1000 cycles, with a capacity retention rate of up to 97.8 %. Fig. 5e presented the charge/discharge voltage distribution of the Zn//MnO_2/CNT cells at different cycles. At the first cycle, the charge and discharge platforms were almost identical, representing the same redox reactions. The capacity of the full batteries assembled with PCA hydrogel electrolytes showed almost no change after 1000 cycles. The specific capacity of ZIBs assembled with LE rapidly decays to 54.3 mAh/g after 200 cycles (Fig. 5f). Meanwhile, the PCA hydrogel electrolytes exhibited virtually no capacity fluctuations during the cycling, retaining a specific capacity of 158.1 mAh/g after 800 cycles with a retention rate exceeding 99 %. These results indicated that the PCA hydrogel electrolytes can significantly enhance the charge/discharge cycling performance of ZIBs, showing good prospects for practical applications.

In summary, we have successfully prepared PCA hydrogel electrolytes with high ionic conductivity and good mechanical properties. In the PCA hydrogel electrolytes, zinc ions are guided and constrained by the carboxy functional groups, inducing uniform deposition of Zn on the (002) crystal surface and suppressing the formation of Zn dendrites. Additionally, the abundance of hydroxyl functional groups in PCA reduce the free water content through hydrogen bonding, altering the solvation structure of Zn^{2+} and inhibiting side reactions. The synergistic effect of these functional groups ultimately promotes uniform and significantly reversible Zn deposition. The excellent mechanical properties of PCA also effectively suppress dendrites growth. Consequently, the lifespan of symmetric Zn//Zn cells extend to 2500 h at the current density of 1.0 mA/cm^2 and the capacity density of 1.0 mAh/cm^2. More impressively, the Zn//MnO_2/CNT full cells maintain a capacity retention rate of 97.8 % after 1000 stable cycles at 1 A/g.

Declaration of competing interest

The authors declare that they have no known competing financial interests or personal relationships that could have appeared to influence the work reported in this paper.

CRediT authorship contribution statement

Yu Wang: Writing – review & editing, Supervision, Data curation. **Kun Ding:** Supervision, Resources, Funding acquisition. **Xuerong Gong:** Validation, Investigation, Conceptualization. **Shou Chen:** Investigation. **Ao Sun:** Investigation. **Junxi Zhang:** Supervision. **Baofeng Wang:** Writing – review & editing, Software, Project administration.

Acknowledgments

This work was supported by the National Natural Science Foundation of China (Nos. 22075173 and 21673136), the Science and Technology Commission of Shanghai Municipality (Nos. 19DZ2271100 and 21010501100) and Shanghai Sailing Program (No. 24YF2714900).

Supplementary materials

Supplementary material associated with this article can be found, in the online version, at doi:10.1016/j.cclet.2025.111078.

References

[1] Y. Gong, B. Wang, H. Ren, et al., Nano-Micro Lett. 15 (2023) 208.
[2] P. Ruan, S. Liang, B. Lu, et al., Angew. Chem. Int. Ed. 61 (2022) e202200598.
[3] H. Zhang, X. Gan, Y. Yan, et al., Nano-Micro Lett. 16 (2024) 106.
[4] J. Lee, H. Lee, C. Bak, et al., Nano-Micro Lett. 15 (2023) 97.
[5] Y. Shang, D. Kundu, Joule 7 (2023) 244–250.
[6] X. Guo, G. He, J. Mater. Chem. A 11 (2023) 11987–12001.
[7] K. Wu, J. Yi, X. Liu, et al., Nano-Micro Lett. 13 (2021) 79.
[8] H. Yu, Z. He, D. Chen, et al., Energy Rev. 4 (2025) 100107.
[9] C. Li, X. Shi, S. Liang, et al., Chem. Engin. J. 379 (2020) 122248.
[10] Q. Zhang, J. Luan, L. Fu, et al., Angew. Chem. Int. Ed. 58 (2019) 15841–15847.
[11] J. Cao, D. Zhang, R. Chanajaree, et al., Adv. Powder Mater. 1 (2022) 100007.
[12] X. Guo, Z. Zhang, J. Li, et al., ACS Energy Lett. 6 (2021) 395–403.
[13] J. Zhou, H. Yu, P. Qing, et al., J. Colloid Interf. Sci. 678 (2025) 772–782.
[14] L. Chen, T. Xiao, J.L. Yang, et al., Angew. Chem. Int. Ed. 63 (2024) e202400230.
[15] X. Wang, M. Yang, Z. Ren, et al., Energy Storage Mater. 70 (2024) 103523.
[16] S. Huang, S. He, Y. Li, et al., Chem. Engin. J. 464 (2023) 142607.
[17] C. Li, X. Jiang, H. Qi, et al., Energy Storage Mater. 75 (2025) 104012.
[18] C. Zhang, C. Li, D. Chen, et al., J. Colloid Interf. Sci. 682 (2025) 232–241.
[19] H. Zheng, Y. Huang, L. Zhao, et al., ACS Sustain. Chem. Eng. 10 (2022) 12751–12762.
[20] R. Ma, Z. Xu, X. Wang, Energy Environ. Mater. 6 (2023) e12464.
[21] S. Zhao, Y. Zuo, T. Liu, et al., Adv. Energy Mater. 11 (2021) 2101749.
[22] Q. He, G. Fang, Z. Chang, et al., Nano-Micro Lett. 14 (2022) 93.
[23] S. Alipoori, S. Mazinani, S.H. Aboutalebi, et al., J. Energy Storage 27 (2020) 101072.
[24] Z. Wang, H. Li, Z. Tang, et al., Adv. Funct. Mater. 28 (2018) 1804560.
[25] A. Mitha, H. Mi, W. Dong, et al., J. Electroanal. Chem. 836 (2019) 1–6.
[26] R. Xu, S. Ma, P. Lin, et al., ACS Appl. Mater. Interfaces 10 (2018) 7593–7601.
[27] H.C. Yu, C.Y. Li, M. Du, et al., Macromolecules 52 (2019) 629–638.
[28] Y. Mao, H. Ren, J. Zhang, et al., Electrochim. Acta 393 (2021) 139094.
[29] E. García-Gaitán, M.C. Morant-Miñana, D. Frattini, et al., Chem. Engin. J. 472 (2023) 144870.
[30] P. Shen, Y. Hu, S. Ji, et al., Colloid. Surf. A: Physicochem. Engin. Asp. 647 (2022) 129195.
[31] P. Xu, C. Wang, B. Zhao, et al., J. Power Sources 506 (2021) 230196.
[32] K. Leng, G. Li, J. Guo, et al., Adv. Funct. Mater. 30 (2020) 2001317.
[33] Z. Zhao, Y. Huang, B. Guo, et al., Chem. Eng. J. 500 (2024) 157431.